JOURNAL OF GEOPHYSICAL RESEARCH, VOL. 111, A11S10, doi:10.1029/2006JA011644, 2006

Kinetic simulations of ring current evolution during the Geospace Environment Modeling challenge events

V. K. Jordanova,[1] Y. S. Miyoshi,[2] S. Zaharia,[1] M. F. Thomsen,[1] G. D. Reeves,[1] D. S. Evans,[3] C. G. Mouikis,[4] and J. F. Fennell[5]

Received 1 February 2006; revised 24 May 2006; accepted 3 August 2006; published 26 October 2006.

[1] We investigate the temporal and spatial evolution of the ring current during two storms selected for study by the Geospace Environment Modeling (GEM) program using our kinetic drift-loss model coupled with a time-dependent plasmasphere model. We use geosynchronous data from LANL satellites to model the inflow of plasma from the magnetotail. We compare results from simulations using either Volland-Stern (VS) or Weimer (W01) model of the convection electric field and investigate the relative effect of magnetospheric convection and radial diffusion on the storm-time injection and trapping of energetic particles and ring current asymmetry. Model comparisons with in situ Cluster, NOAA, and Polar energetic particle observations show overall better agreement with W01 than with VS model. On the other hand, VS model reproduced better the evolution of the plasmapause as observed by IMAGE. Additional ring current ion injections caused by radial diffusion near *Dst* minima improved the agreement with observations. Radial diffusion did not affect much ring current buildup during the main phase of the storms and the ring current fluxes remained asymmetric, in good agreement with NOAA data. We calculated the excitation of electromagnetic ion cyclotron (EMIC) waves self-consistently with the evolving plasma populations, and the resulting precipitating fluxes of resonant protons. These fluxes increased significantly within regions of enhanced plasma wave excitation near the plasmapause or inside plasmaspheric plumes and reduced the total H^+ energy by $\sim$10% during the storm recovery phase. Initial results from self-consistent magnetic field calculations are presented as well. We found that while the magnitude of the ring current fluxes was reduced when adiabatic drifts in a self-consistent magnetic field were calculated, their morphology was not affected significantly and the local time of the equatorial flux peaks remained almost unchanged.

Citation: Jordanova, V. K., Y. S. Miyoshi, S. Zaharia, M. F. Thomsen, G. D. Reeves, D. S. Evans, C. G. Mouikis, and J. F. Fennell (2006), Kinetic simulations of ring current evolution during the Geospace Environment Modeling challenge events, *J. Geophys. Res.*, *111*, A11S10, doi:10.1029/2006JA011644.

1. Introduction

[2] In recent years the relations between the energy output from the Sun and the subsequent magnetic activity at Earth are being investigated in great detail. Of central interest are the dynamics of the inner magnetosphere where most of the solar wind energy is deposited and dissipated. As more sophisticated technologies are placed into space-affected systems, there is an increasing need for better understanding of the geospace environment. The goals are to develop predictive models of energetic particle dynamics and electrical current systems and to be able to forecast adverse activity that could be dangerous to technologies and humans in space.

[3] In the inner magnetosphere, plasma does not behave as a fluid, and numerical kinetic simulations of particle dynamics are the primary tool to study geomagnetic storms. Numerical models of ring current evolution were developed using various computational methods [e.g., *Kistler et al.*, 1989; *Fok et al.*, 1993; *Chen et al.*, 1994; *Jordanova et al.*, 1994] and have improved our understanding of storm dynamics. The inner magnetosphere models are now becoming very complex, even including coupling with ionospheric regions. One of the present challenges is to develop ring current models that calculate self-consistently the electric and magnetic fields in which the particles drift. Ring current parameters during the 12 August 2000 storm

[1]Los Alamos National Laboratory, Los Alamos, New Mexico, USA.
[2]Solar-Terrestrial Environment Laboratory, Nagoya University, Nagoya, Japan.
[3]Space Environment Center, NOAA, Boulder, Colorado, USA.
[4]Space Science Center, University of New Hampshire, Durham, New Hampshire, USA.
[5]Aerospace Corporation, Los Angeles, California, USA.

0148-0227/06/2006JA011644$09.00

obtained with the ring current model of *Fok et al.* [2001] coupled with the Rice Convection Model (RCM) [*Wolf et al.*, 1982; *Toffoletto et al.*, 2003], reproduced well the postmidnight enhancements of the proton fluxes observed with the HENA instrument on the Imager for Magnetopause-to-Aurora Global Exploration (IMAGE) satellite [*Ebihara and Fok*, 2004]. The RCM calculates the potential electric field self-consistently by solving the fundamental equations of magnetosphere-ionosphere coupling, assuming a multispecies plasma with isotropic pitch angle distributions; initial studies considering coupling with models that supply theoretically computed magnetic fields have been performed [*Lemon et al.*, 2004; *De Zeeuw et al.*, 2004], but self-consistent calculation of the magnetic field in force balance with anisotropic plasma distributions has not been implemented. Self-consistently calculated electric and magnetic fields will affect the evolution of the plasmasphere as well. The dependence of the plasmaspheric morphology on the electric field description was investigated by *Liemohn et al.* [2004] during the recovery phase of the 17 April 2002 storm. They showed that both the *Weimer* [1996] model and a self-consistent potential model [*Ridley et al.*, 2004] provide a good description of the storm-time development of the plasmasphere, with the self-consistent electric field model being the best choice. Additional complexity in calculating ring current distributions comes from the necessity of simulating the losses due to collisions and wave-particle interactions with the ambient neutral and plasma environment. Another challenge therefore is the development of a self-consistent treatment of particle transport and wave instabilities. Such an approach has been used in our ring current-atmosphere interactions model (RAM) [*Jordanova et al.*, 2001a, 2003] to show the effectiveness of electromagnetic ion cyclotron (EMIC) waves in causing ion precipitation.

[4] We have recently expanded our kinetic RAM model to include diffusive transport and study the dynamics of particles at relativistic energies [*Jordanova and Miyoshi*, 2005]. In this investigation we use our model to simulate ring current ion dynamics during two storms selected for detailed study by the Inner Magnetosphere-Storm (IMS) campaign of the Geospace Environment Modeling (GEM) program at the National Science Foundation (NSF). These storms occurred on 22 April 2001 and on 21 October 2001. The goal of the GEM/IMS Challenge is to assess (1) the accuracy of various models to predict realistically inner magnetosphere dynamics during magnetic storms, and (2) our understanding of the physical processes occurring in the near-Earth space environment. We compare the relative effect of magnetospheric convection, radial diffusion, and wave-particle interactions on ring current evolution. We use two different models of inner magnetospheric convection, the Volland-Stern [*Volland*, 1973; *Stern*, 1975] model and the Weimer [*Weimer*, 2001] model, both to show the sensitivity of RAM to the electric field model description and to highlight strengths and weaknesses of these convection models. Initial results from the further adaptation of RAM to more realistic nondipole magnetic field configurations and the addition of a self-consistent calculation of the magnetic field are presented as well. The accuracy of the RAM model to simulate the dynamics of relativistic electrons during the October 2001 storm and new physical insights gained are discussed in a companion paper by *Miyoshi et al.* [2006].

2. Observations

2.1. Interplanetary Data

[5] Measurements of solar wind plasma [*McComas et al.*, 1998] and interplanetary magnetic field (IMF) [*Smith et al.*, 1998] from the Advanced Composition Explorer (ACE) during the storm periods under investigation are shown in Figure 1. The interplanetary data are delayed with an appropriate time (i.e., ~60 min during the April storm and ~40 min during the October storm) to account for signal propagation to Earth. An interplanetary shock was observed on 21 April at hour ~16 (Figure 1, left). Behind the shock, the density, dynamic pressure, and total field increased, and the solar wind speed reached values of ~400 km/s. At hour ~25, ACE entered a region with strong and smooth fields and a relatively smooth south-to-north B_z excursion characteristic of a magnetic cloud. The IMF B_z component decreased to about −15 nT at hour ~35 and began a slow northward rotation thereafter. The polar cap potential derived from the *PC* index using the empirical relation of *Troshichev et al.* [1996] increased gradually after hour 24 and reached a maximum of ~140 kV at hour 34.5. The magnetic cloud triggered a moderate geomagnetic storm at Earth with a ~15-hour-long main phase, minimum $Dst = -102$ nT at hour 40, maximum $Kp = 6^+$, and a storm recovery lasting more than a day.

[6] The large geomagnetic storm of 21 October 2001 (Figure 1, right) had a rapid main phase reaching minimum $Dst = -187$ nT and maximum $Kp = 8^-$ at approximately hour 22, followed by a ~28-hour-long period of strong geomagnetic activity. The storm was triggered by the sheath of a magnetic cloud at hour ~16 when the associated interplanetary shock reached the Earth. The IMF B_z component showed large fluctuations within the sheath region and decreased to about −20 nT, while the solar wind speed increased to ~700 km/s. The polar cap potential had maximum values of about 195 kV and 200 kV at hour ~18 and hour ~24, respectively. The IMF B_z reached a second negative excursion of about −15 nT within the magnetic cloud at hour ~33, a maximum $Kp = 7^+$ was recorded at hour 39, and the polar cap potential peaked to ~175 kV at hour 42.5. A second minimum $Dst = -165$ nT occurred at hour 49, followed by a slow storm recovery lasting for several days.

2.2. Magnetospheric and Ionospheric Data

[7] In this study we use energetic particle observations from the following satellites: the Los Alamos National Laboratory (LANL) spacecraft at geosynchronous orbit, the low-altitude orbiting National Oceanic and Atmospheric Administration (NOAA) spacecraft, and the Cluster, Polar, and IMAGE spacecraft on elliptical orbits around the Earth. The geosynchronous data are used to provide realistic boundary conditions for our model, while data from the other satellites are used for initial conditions and for comparisons with model simulations.

[8] Ion fluxes from the Magnetospheric Plasma Analyzer (MPA) [*McComas et al.*, 1993] in the energy range 1 eV–40 keV, and the Synchronous Orbit Particle Analyzer

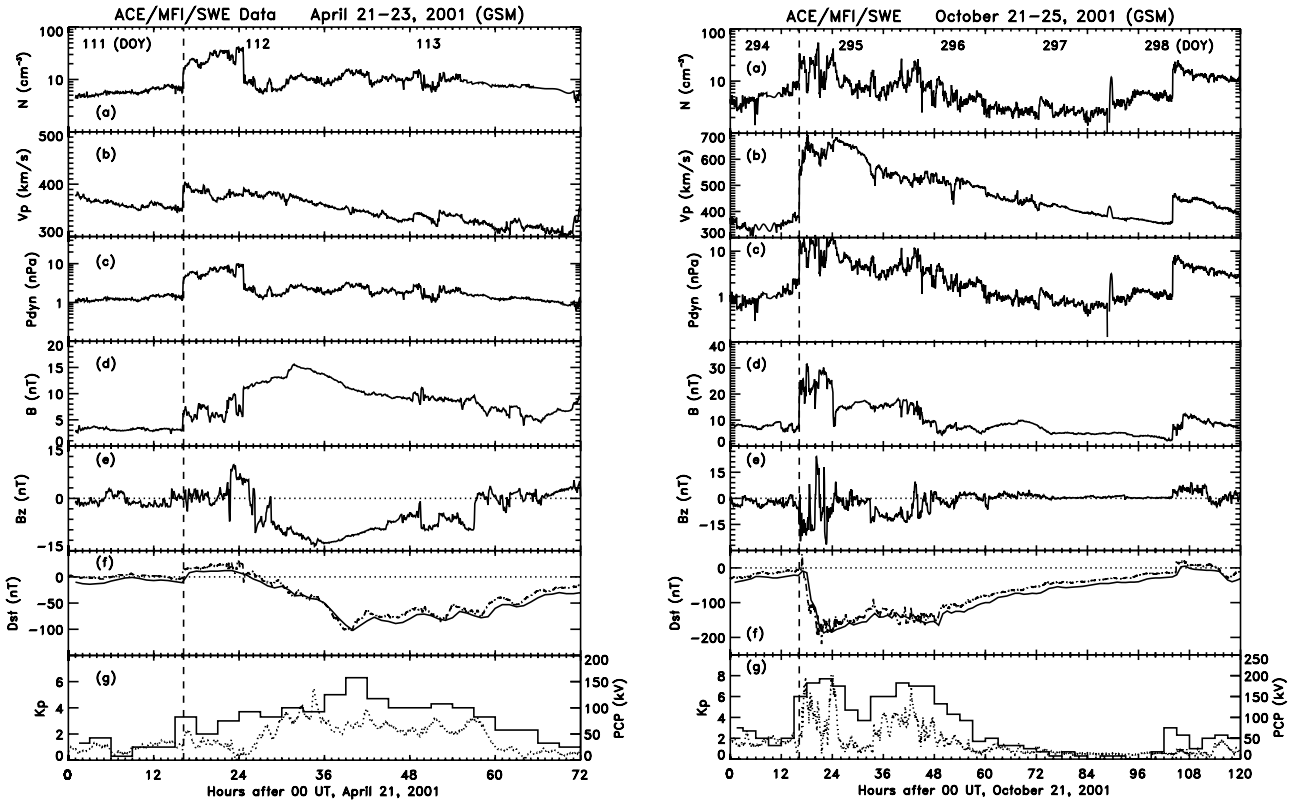

Figure 1. (left) Interplanetary observations from the MFI and SWEPAM instruments on ACE during 21–23 April 2001. From top to bottom the panels are proton density, solar wind bulk speed, solar wind dynamic pressure, magnetic field strength, the B_z (GSM) component of the magnetic field, the measured *Dst* (solid) and SYM-H (dash-dotted) indices, the planetary *Kp* index (solid) and the polar cap potential (dotted line). (right) Interplanetary observations during 21–25 October 2001. The vertical dashed line indicates the interplanetary shock driven by the magnetic cloud. The day of the year (DOY) is given in the top panel for reference.

(SOPA) [*Belian et al.*, 1992] (energy >50 keV) instruments on LANL satellites 080, 084, and 01A were available during both storm periods. These satellites were located at about 90° separation in longitude and provided very good coverage of the time-varying conditions at geosynchronous orbit in response to solar wind changes. The plasma sheet ion density (computed in the energy range of ~100 eV to 40 keV) increased significantly on the nightside during the main phase of the storms, reaching values of ~2 cm^{-3} during the April storm and up to 3 cm^{-3} during the October storm, then returning to normal values during the storm recovery phases. During the October storm there was an additional plasma sheet density enhancement near the second *Dst* minimum, however of smaller (~1.5 cm^{-3}) magnitude. The MPA instrument measures the plasmaspheric ion density (in the energy range ~1 eV to 100 eV) at geosynchronous orbit as well. The LANL observations indicated the traversals of a dayside plasmaspheric plume (cold plasma density >10 cm^{-3}) from ~0500 until ~1600 UT in the afternoon sector (1230–1900 MLT) on 22 April, from ~0300 until ~1400 UT (1600–1900 MLT) on 21 October, and from ~0100 until ~1400 UT (1100–1700 MLT) on 22 October.

[9] Measurements from the Medium Energy Proton and Electron Detector (MEPED) [*Evans and Greer*, 2000] on board the NOAA-15 satellite during 21–23 April and 21–24 October 2001 are shown in Figure 2. The NOAA-15 satellite has an orbit at ~830 km altitude in the dusk-dawn (~1900–0700 LT) meridian plane. The data are plotted as an *L*-time diagram, where *L* is the McIlwain parameter calculated with the IGRF-2000 model propagated forward in time to epoch 2001.5. The MEPED instrument makes observations in two directions, roughly vertical (the 0° telescope) and roughly horizontal (the 90° telescope). Ion data (there is no ion mass separation) from the three lowest-energy channels of the 90° telescope are displayed. These correspond to trapped particles (local pitch angle $\alpha \geq 75°$) at high latitudes and to particles with local pitch angle $\alpha \leq 60°$ at low latitudes. The corresponding equatorial pitch angles estimated from the IGRF model are $\alpha_o \geq 6°$ at $L = 4$ and $\alpha_o \leq 18°$ at $L = 2$; therefore at lower latitudes the MEPED detector is observing particles at pitch angles in the local atmospheric loss cone and the count rates are very small. The black line in each panel indicates the instantaneous plasmapause location calculated from *O'Brien and Moldwin* [2003] as a function of the *Kp* index.

[10] Intense enhancements of 30–80 keV ions were observed near *Dst* minima of both storms on the duskside (Figure 2b); the flux was about two orders of magnitude smaller on the dawnside (Figure 2a). The maximum ion flux

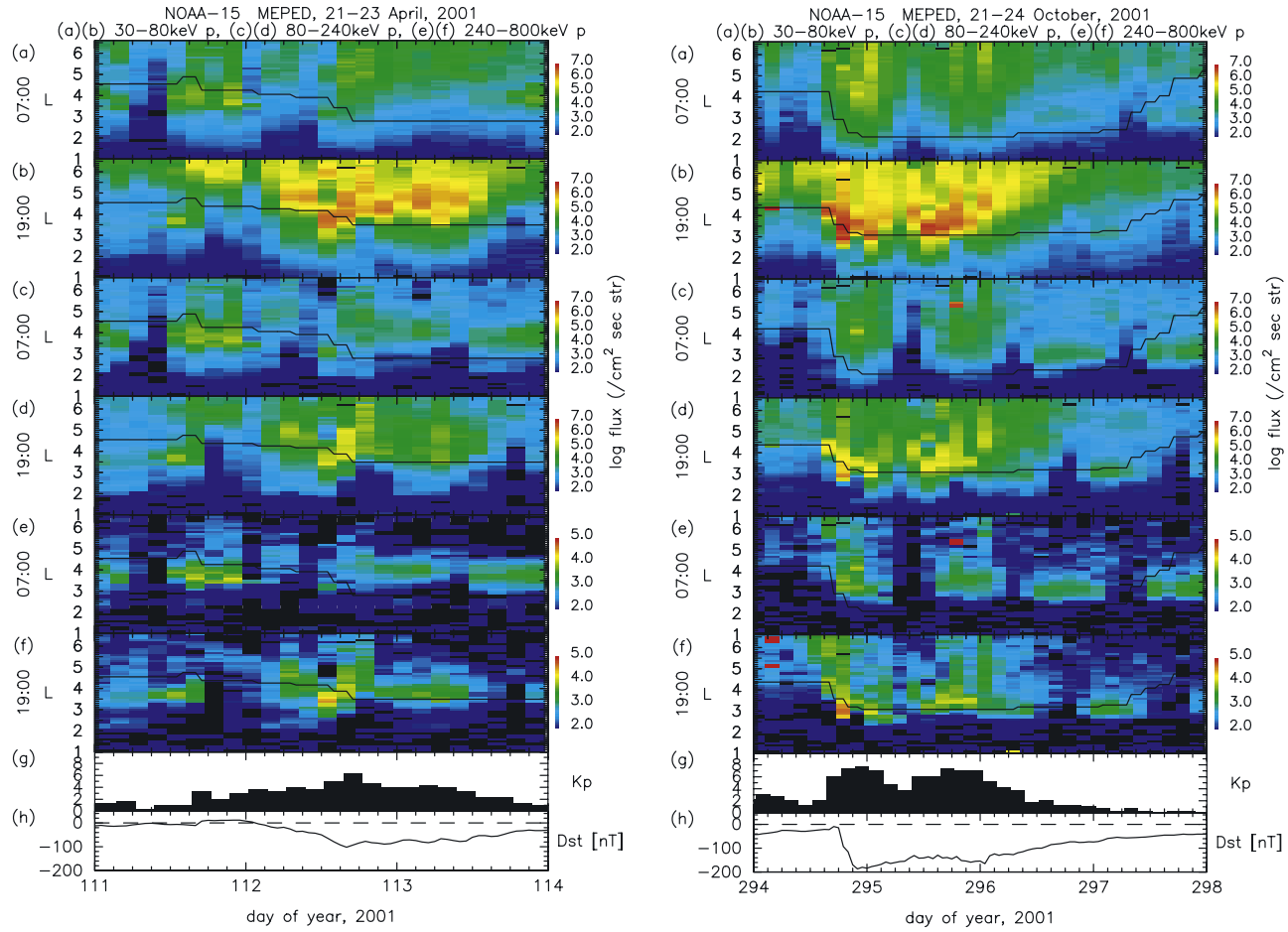

Figure 2. (left) Fluxes (1 cm^{-2} s^{-1} str^{-1}) of locally mirroring ions measured with the MEPED instrument on NOAA during 21–23 April, 2001. From top to bottom the panels are 30–80 keV ion fluxes at (a) LT = 0700 and (b) LT = 1900; 80–240 keV ion fluxes at (c) LT = 0700 and (d) LT = 1900; 240–800 keV ion fluxes at (e) LT = 0700 and (f) LT = 1900; (g) the *Kp* index; and (h) the measured *Dst* index. (right) NOAA observations during 21–24 October, 2001. The black color bins correspond to periods of very low count rates or missing data. The black line indicates the instantaneous plasmapause location.

occurred at times when maximum *Kp* and minimum *Dst* were recorded. Ion fluxes in the 30–80 keV energy range from NOAA-16 satellite (not shown) exhibited similar asymmetry, being more intense at LT = 0200 (of the order 10^6 $cm^{-2}s^{-1}str^{-1}$ on 22 April and of the order 10^7 $cm^{-2}s^{-1}str^{-1}$ on 21 October) than at LT = 1400 (of the order 10^5 $cm^{-2}s^{-1}str^{-1}$ on 22 April and of the order 10^6 $cm^{-2}s^{-1}str^{-1}$ on 21 October). The flux decreased as geomagnetic activity decreased, and the plasmapause retreated to higher *L* shells during the later storm recovery. Similar trends were observed in the higher-energy channels; however, the flux was about an order of magnitude smaller in the 80–240 keV range (Figures 2c and 2d) and about two orders of magnitude smaller in the 240–800 keV range (Figures 2e and 2f). The highest energy MEPED flux, being less responsive to the enhanced convection electric field, was much less asymmetric in LT than the fluxes at lower energies.

[11] Data from an inner magnetosphere pass of the Cluster Ion Spectrometry (CIS) experiment [*Rème et al.*, 2001] on Cluster were available from ~2000 to 2400 UT on 21 October 2001. At this time Cluster perigee was near the magnetic equatorial plane in the dayside magnetic local time sector (MLT ~ 0900). CIS measures the three-dimensional distribution functions of the major ring current ion species, H^+, He^+, and O^+ over the energy per charge range 20–40,000 eV/e. Near 2300 UT on 21 October 2001, the CIS energy spectra [*Jordanova et al.*, 2005] clearly showed the deep stagnation minimum at about 10 keV at $L \sim 5$ in all species due to the slow ion drift velocity at this energy [e.g., *Lennartsson et al.*, 1979; *Jordanova et al.*, 2001b]. Near 2100 UT, low-energy heavy ion ionospheric outflows were observed at ~80° invariant latitude. In the inner magnetosphere, at high energies H^+ distribution peaked at 90° pitch angle, while at low energy O^+ and He^+ had field-aligned distributions.

[12] In situ energetic particle data in the inner magnetosphere were provided as well from the instruments on Polar spacecraft. In this study we use observations from the Magnetospheric Ion Composition Sensor (MICS) [*Wilken et al.*, 1992] which measures H^+, O^+, He^+, and other minor ion distributions in the energy range from 1 keV to 200 keV.

During 21–25 October 2001 the orbit of Polar satellite was approximately in the noon-midnight meridian (MLT = 1000–2200), with perigee in the prenoon local time sector and apogee near the equator at $L \sim 10\ R_E$ on the nightside. All near-equatorial data at $L < 6$ were taken near perigee where Polar was moving at high velocity and good spatial resolution could not be obtained. Therefore MICS fluxes were available near the magnetic equator only at distances from Earth with $L > 6$ on the nightside. In addition, global observations of the inner magnetosphere were provided by the instruments on board the IMAGE satellite. The Extreme Ultraviolet (EUV) imager [*Sandel et al.*, 2001] obtains images of the plasmasphere with a lower sensitivity threshold equivalent to total ion density of $\sim$40 cm^{-3}. During 21–23 April 2001 the global images indicated storm-time features like plasmaspheric erosion and formation of a dayside plume of sunward flowing plasma [*Goldstein et al.*, 2005] in agreement with LANL observations of a dayside plume mentioned above. Comparisons of simulation results from our model with data from these spacecraft are discussed in section 4.

3. Model Description

[13] We investigate ring current dynamics during the April and October 2001 geomagnetic storms using our global ring current-atmosphere interactions model (RAM) briefly summarized below (for further details, see *Jordanova et al.* [1996a, 2003]). The model evaluates numerically the bounce-averaged kinetic equation for the distribution function $Q_l(R_o, \phi, E, \mu_o, t)$ for species l in the magnetic equatorial plane. All three major ring current ion species H^+, O^+, He^+, and electrons are included in our model. In order to study the dynamics of both ring current and radiation belt particles, a combined convection-diffusion approach is used [*Jordanova and Miyoshi*, 2005] and the relativistic kinetic equation is solved:

$$\frac{\partial Q_l}{\partial t} + \frac{1}{R_o^2}\frac{\partial}{\partial R_o}\left(R_o^2\left\langle\frac{dR_o}{dt}\right\rangle Q_l\right) + \frac{\partial}{\partial\phi}\left(\left\langle\frac{d\phi}{dt}\right\rangle Q_l\right) + \frac{1}{\gamma p}\frac{\partial}{\partial E} \cdot \left(\gamma p\left\langle\frac{dE}{dt}\right\rangle Q_l\right) + \frac{1}{h(\mu_o)\mu_o}\frac{\partial}{\partial\mu_o}\left(h(\mu_o)\mu_o\left\langle\frac{d\mu_o}{dt}\right\rangle Q_l\right) = \left\langle\left(\frac{\partial Q_l}{\partial t}\right)_{rd}\right\rangle + \left\langle\left(\frac{\partial Q_l}{\partial t}\right)_{loss}\right\rangle. \quad (1)$$

The phase space volume element is given by $dV = 8\pi m_o \gamma p R_o^2 \mu_o h(\mu_o) dR_o d\phi dE d\mu_o$. Here p is the relativistic momentum of the particle and $h(\mu_o) = S_B/(2R_o)$, where S_B is the half-bounce path length. The relativistic factor $\gamma = 1 + E/(m_o c^2)$, where m_o is the rest mass, E is the kinetic energy of the particle, and c is the speed of light. The model includes radial distances in the equatorial plane R_o from 2 R_E to 6.5 R_E and all magnetic local times, kinetic energy E from 100 eV to 800 keV, and equatorial pitch angle α_o from 0° to 90°, where μ_o is the cosine of α_o. The grid sizes for radial distance and magnetic local time are 0.25 R_E and 1 hour, respectively. The energy grid is defined as $\delta E_i/\delta E_{(i-1)} \sim 1.3$ and the pitch angle grid separation is approximately 1°. The brackets $\langle\ \rangle$ denote bounce-averaging and the index o refers to the quantities in the equatorial plane. The time-dependent boundary conditions on the nightside are determined from plasma sheet flux measurements by the LANL spacecraft at geosynchronous orbit, using the *Young et al.* [1982] study to correlate the ion composition with geomagnetic and solar activity, and preserving the local time dependence of the data [*Jordanova et al.*, 2001a]. The boundary conditions on the dayside correspond to free ion outflow.

[14] The left-hand side of equation (1) describes the adiabatic drift of charged particles, while the right-hand side describes changes of Q_l due to losses and diffusive transport. Particle drifts at ring current energies are determined by the magnitudes of the $\mathbf{E} \times \mathbf{B}$ and the magnetic gradient-curvature velocities. An essential quantity in modeling ring current dynamics is therefore the convection electric field. We have developed our ring current model so that an arbitrary electric field $\mathbf{E}$ model could be used as a driver. When an ionospheric potential model is used, the ionospheric potentials are mapped to the Solar Magnetic (SM) equatorial plane using the IMF- and *Dst*-driven magnetic field model of *Tsyganenko* [2002] and the electric potentials are obtained as a function of radial distance in the equatorial plane and MLT [*Jordanova et al.*, 2001b, 2003]. In this study we compare results from an analytical convection model [*Volland*, 1973; *Stern*, 1975; *Maynard and Chen*, 1975] and an empirical ionospheric model [*Weimer*, 2001]. The corotation potential is kept the same in both approaches: $U_{cor} = -C/R_o$, where C is the corotation constant.

[15] The RAM model includes all major loss processes of ring current ions: charge exchange, Coulomb collisions, wave-particle interactions, and loss due to collisions with the dense atmosphere (for more details, see *Jordanova et al.* [1996a, 2001a]). Our model is coupled with the time-dependent plasmasphere model of *Rasmussen et al.* [1993], which calculates the thermal electron density in the equatorial plane by following the motion of individual flux tubes. Changes in the total flux tube content are due to the ionospheric supply and loss and flux tube volume changes caused by the $\mathbf{E} \times \mathbf{B}$ drift. A dipolar magnetic field and a traditional Volland-Stern convection and corotation model were originally used in the plasmasphere model. We have now implemented the empirical convection model of *Weimer* [2001] in the plasmasphere model and present results from these coupled models for the April and October 2001 storms. Scattering of ring current ions by plasma waves is implemented self-consistently in RAM by calculating the equatorial growth rate of EMIC waves from the hot plasma dispersion relation solved simultaneously with the kinetic equation (1). We integrate the local growth rates along wave paths to obtain the wave gain and calculate the wave amplitudes using an empirical relation [*Jordanova et al.*, 2003]. The effect of wave-particle interactions on ring current ion distributions is treated in the ring current model following quasi-linear theory as a diffusive process, and the multi-ion diffusion coefficients of *Jordanova et al.* [1996b] are used. Since pitch angle diffusion rates are usually faster than energy diffusion rates, only pitch angle diffusion is considered in this study.

[16] We have recently extended our ring current model to solve the kinetic equation for the electron distribution function [*Jordanova and Miyoshi*, 2005]. To include the diffusive transport of relativistic particles, as a result of fast

electric and magnetic field ULF fluctuations, we added a radial diffusion term [e.g., *Schulz and Lanzerotti*, 1974] to the right-hand side of the equation (1):

$$\left\langle \left(\frac{\partial Q_l}{\partial t}\right)_{rd} \right\rangle = R_o^2 \frac{\partial}{\partial R_o}\left[\frac{1}{R_o^2}\langle D_{R_oR_o}\rangle \frac{\partial Q_l}{\partial R_o}\right]_{(M,J)}. \quad (2)$$

Here $D_{RoRo} = R_E^2 D_{LL}$ and M and J are the first and second adiabatic invariants. In this study we use the *Kp*-dependent radial diffusion coefficients D_{LL} from the empirical analysis of *Brautigam and Albert* [2000]. We consider only magnetic diffusion, as the dominant diffusive process [*Shprits and Thorne*, 2004], and to avoid double-counting of the effects of time-varying electric fields.

[17] Finally, a dipolar magnetic field approximation was implemented at first in our kinetic model [e.g., *Jordanova et al.*, 1994]. Most of the results presented in this study still employ a dipolar model of the magnetic field of the Earth, except for the electric potential mapping discussed above. However, it is clear that such an approximation excludes such important physical processes that occur in the real magnetospheric field as drift shell splitting [*Sibeck et al.*, 1987], the effects being more pronounced at larger L shells. In addition, the ring current buildup during the main phase of a storm induces a magnetic field in an opposite direction to the terrestrial magnetic field and thus significantly modifies the field [e.g., *Tsyganenko*, 2002; *Zaharia et al.*, 2005] and the storm-time particle drifts. Therefore we are including a more realistic, self-consistent, magnetic field treatment in our model and present initial results in section 4.4 of this paper. The anisotropic pressure calculated with our ring current model is used as input for a 3-D equilibrium code [*Zaharia et al.*, 2004] and the force-balanced magnetic field is computed at 1-hour time intervals. The newly calculated magnetic field (interpolated between the 1-hour intervals) is then used in RAM to update the particle drifts. The iteration is repeated until the solution converges. Details of this calculation, as well as additional self-consistent physical results for the April 2001 storm are discussed in a companion paper of *Zaharia et al.* [2006]. We note that the inductive electric field due to the time-changing **B** field is not yet included in the coupled model. Its inclusion, however, will be greatly facilitated by the Euler potential representation of the **B** field in the 3-D equilibrium code and will be considered in the future.

[18] Our approach to incorporate a nondipolar magnetic field representation differs from that of previous authors [e.g., *Fok et al.*, 2001] who solved the kinetic equation at ionospheric altitudes so they could still apply the dipolar approximation, obtaining the distribution in the equatorial plane by mapping along prescribed realistic magnetic field lines. We retain the solution of the kinetic equation in the magnetic equatorial plane, using the form of the bounce-averaged gradient-curvature drift [*Roederer*, 1970] valid for realistic magnetic field models which include external electric currents [*Shukhtina*, 1993]:

$$\langle \vec{V}_{GC} \rangle = \frac{2p}{q\tau_B B_o} \nabla_o I \times \vec{e}_o. \quad (3)$$

[19] The $\mathbf{E} \times \mathbf{B}$ drift in the equatorial plane of an arbitrary magnetic field is

$$\langle \vec{V}_{conv} \rangle = \frac{\vec{E}_o \times \vec{B}_o}{B_o^2}. \quad (4)$$

The purely field-geometric integrals $S_B = \int ds/\sqrt{(1 - B(s)/B_m)}$ and $I = \int ds\sqrt{(1 - B(s)/B_m)}$ are calculated for the realistic **B** field, along the field lines and between the mirror points where the field intensity is B_m. In this initial study the bounce-averaging of the loss terms is still calculated in a dipole field, so the final results will be modified once this is updated in the code. To estimate the magnitude of this uncertainty, we note that during geomagnetically active conditions the bounce-averaged geocoronal hydrogen density for the nondipole magnetic field model of *Tsyganenko* [2002] differed little from the quantities calculated in a dipole field, except in the dusk-midnight sector where the difference was ~20% [*Vapirev and Jordanova*, 2005]. We expect additional changes to occur when the RAM code is fully coupled with the 3-D equilibrium code and the solution is updated at smaller than 1-hour time steps, and when the inductive electric field is included. These aspects will be investigated in future extensions of this work.

4. Comparison of Model Results With Observations

4.1. Convection Electric Field and Plasmasphere Evolution

[20] We studied ring current ion evolution during the geomagnetic storms of April and October 2001 using our kinetic RAM model driven by two different models of the convection electric field. The first, Volland-Stern (VS) convection model has a simple analytical form and is derived as the gradient of the potential $U_{conv} = AR_o^{\chi}\sin(\phi)$. In this study we used a shielding factor $\chi = 2$ and a parameter A as a function of geomagnetic activity through the *Kp* index [*Maynard and Chen*, 1975]; we interpolated between the 3-hour averaged *Kp* values to obtain a smooth solution. The second, *Weimer* [2001] (W01) convection model is an empirical model derived from measurements of the Vector Electric Field Instrument (VEFI) on the DE 2 spacecraft and depends on the interplanetary conditions. As inputs to this model, we used the IMF and solar wind data from ACE (Figure 1). We mapped the ionospheric patterns to the magnetic equator using the *Tsyganenko* [2002] magnetic field model and assuming equipotential field lines.

[21] Both models predicted that a stronger electric field penetrated to lower L shells during the October storm than during the April storm. The cross polar cap potential drop reached maximum approximately at the same time near 2400 UT on 21 October in both VS and W01 models; however, on 22 April it maximized near 1100 UT in W01, and 5 hours later near 1600 UT in VS (see discussion in section 4.2). The potential patterns (not shown) are symmetric by definition in the VS model, while they exhibit significant local time asymmetry and small-scale structures in the Weimer model [*Jordanova et al.*, 2001b]. The W01 model predicted larger fields on the duskside and closer to Earth than the VS model during the main phase of both

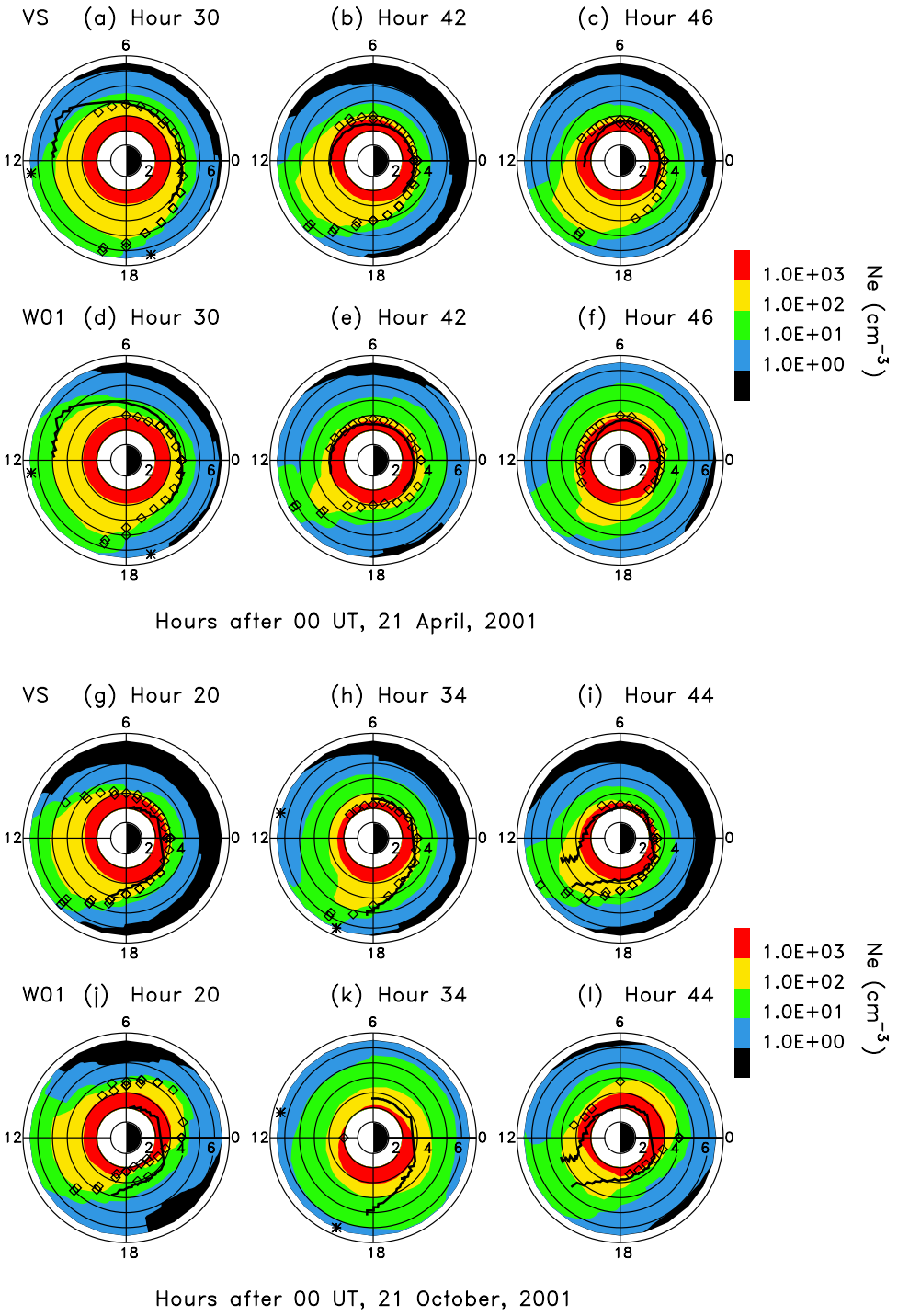

Figure 3. (a through f) Equatorial plasmaspheric electron densities (cm^{-3}) at selected hours after 0000 UT, 21 April 2001, (top) using Volland-Stern (VS) convection model, and (bottom) using Weimer (W01) convection model. (g through l) Equatorial plasmaspheric electron densities at selected hours after 0000 UT, 21 October 2001. The plasmapause location determined from IMAGE/EUV data is plotted with a solid line. The locations where LANL satellites observed cold ion density above 10 cm^{-3} are shown with stars. The diamonds indicate the plasmapause as determined from our model simulations.

storms. Cluster Electron Drift Instrument (EDI) and Electric Field and Wave (EFW) data on 21 October 2001 were compared with the W01 model by *Jordanova et al.* [2005]. The radial component of the model showed good agreement with the 10-min averaged radial component of the merged EDI and EFW electric fields. However, there were significant differences between the two azimuthal components, the model being stronger than the data near 2300 UT and weaker near 2330 UT. The Cluster data indicated a large ULF (Pc 5) wave component as well.

[22] We simulated the evolution of the plasmaspheric electron density and showed the results at selected hours

after 0000 UT, 21 April in Figures 3a through 3f. Simulations using the Volland-Stern convection model are shown in the top panels, while simulations using the Weimer convection model are shown in the bottom. Respective plasmaspheric simulations after 0000 UT, 21 October are shown in Figures 3g through 3l. Initially, during periods of low geomagnetic activity (Figures 3a and 3d) the plasmasphere was more symmetric in local time and extended to $L \sim 4.5$ on the nightside. On the dayside, densities larger than 10 cm^{-3} were predicted in the afternoon sector from ~1200 to 1700 MLT at geosynchronous orbit in agreement with a broad dayside plume observed by LANL satellites. With increasing geomagnetic activity (Figures 3b, 3e, 3g, and 3j), the plasmasphere eroded and higher densities were confined to lower L shells and to the dayside afternoon plume. As geomagnetic activity decreased, the plume corotated moving toward dusk (Figures 3f and 3h). The plasmapause location determined from IMAGE/EUV data [*Goldstein et al.*, 2005] is plotted in Figure 3 with a solid line; it indicates the location of a steep gradient in electron density or, in the case of IMAGE data, a density drop below the sensitivity threshold of the instrument. The plasmapause identified from our model as the region where the thermal density drops by a factor of 5 or more over a distance of 0.25 R_E is shown with diamonds. Both VS and W01 models reproduced very well the plasmapause location during quieter times and during the April storm (Figures 3a through 3f). During active times both models predicted the plasmapause position at slightly larger L shells than IMAGE, but the difference is close to the subjective uncertainty in the EUV plasmapause. The W01 model reproduced better the formation of the plume in the postnoon sector (Figures 3e and 3f). During the October storm, however, the VS model (Figures 3g, 3h, and 3i) reproduced significantly better the plasmapause location than the W01 model (Figures 3j, 3k, and 3l). During the late storm recovery, the plasmasphere refilled and the plasmapause receded back to larger L shells (not shown).

4.2. Ring Current Evolution

[23] We compared ring current ion buildup caused by magnetospheric convection and radial diffusion during the April and October storms in Figures 4 and 5, respectively. The top panels show the cross polar cap potential (CPCP) drop, obtained with the VS (dashed) and W01 (dash-dotted) models and derived from the polar cap index using the empirical equation of *Troshichev et al.* [1996] (solid). The corresponding ring current injection rate obtained with RAM (defined as the total energy gain per hour) is shown in the middle panels. The *Dst* index computed using the Dessler-Parker-Sckopke relation (including currents induced in the diamagnetic Earth [*Dessler and Parker*, 1959; *Sckopke*, 1966]) is compared with measured *Dst* in the bottom panels. During 22 April the CPCP drop calculated with W01 (Figure 4) rose quickly and reached maximum ~120 kV at hour ~35, while the CPCP drop calculated with the VS model peaked about 5 hours later when the *Kp* index had maximum values (see Figure 1). The calculated W01 CPCP agreed reasonably well with the Troshichev et al. CPCP values. The ring current injection rate reflected the changes of the convection potential and the inflow of plasma at the nightside boundary. It increased

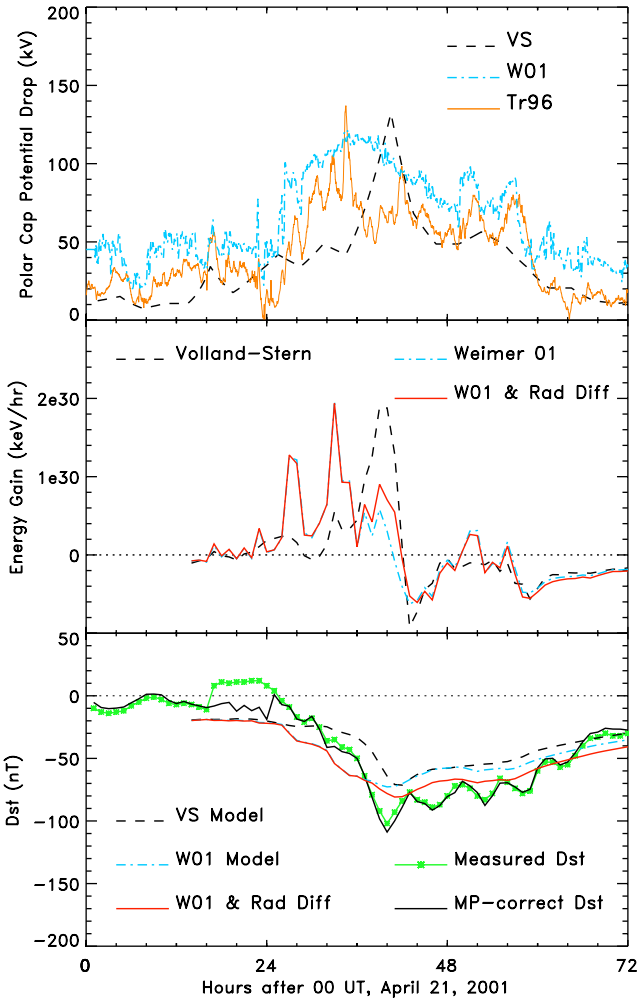

Figure 4. (top) Polar cap potential drop obtained with the *Kp*-dependent Volland-Stern model (dashed line), the IMF-dependent model of Weimer (dash-dotted line), and from the *PC* index (solid line, after *Troshichev et al.* [1996]). (middle) Ring current injection rate calculated with the Volland-Stern model (dashed), Weimer model (dash-dotted), and Weimer model and radial diffusion (solid). (bottom) Computed *Dst* index using the three model formulations compared with measured *Dst* (starred line) and magnetopause current-corrected *Dst* (dash-dot-dotted line) during 21–23 April 2001.

significantly using W01 near hours 27 and 33, causing considerable ring current intensification. Additional enhancements of the convection potential occurred during the recovery phase near hours 50 and 56 and caused smaller increases in the injection rate at these times. The magnetic field disturbance of the ring current on ground reached minimum near hour 40 and slowly decayed thereafter. We note that the solar wind dynamic pressure was small during 21–23 April, and the magnetopause currents corrections to *Dst* were negligible. The VS model predicted different ring current behavior during this storm; the injection rate started to increase at hour ~32 and peaked near hour 40, causing minimum *Dst* at hour 42. Both the VS and W01 models underestimated *Dst* minimum during the April storm by ~30 nT. Better agreement was obtained when the process of

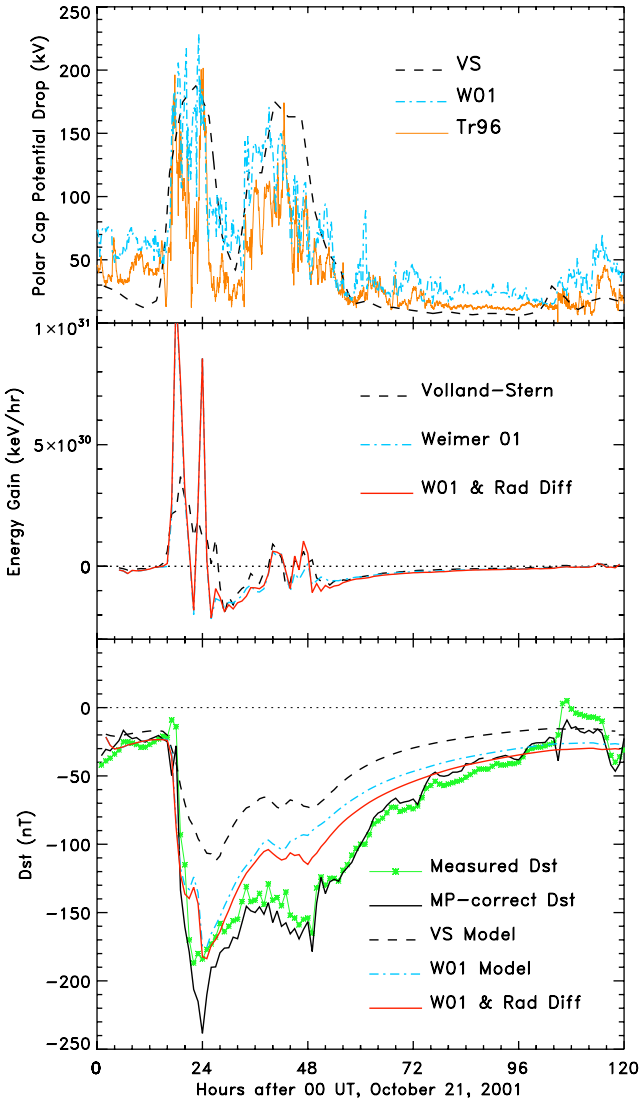

Figure 5. Model simulations and data during 21–25 October 2001 in the same format as Figure 4.

radial diffusion due to magnetic field fluctuations was included; the RAM simulations using the W01 convection model and radial diffusion are shown with solid line in the middle and bottom panels. Radial diffusion produced an additional injection of ring current ions at hour ~39 and about 15% enhancement of ring current energy at hour 42 (Figure 4). The ring current decayed during the storm recovery phase due to the loss processes, which were kept the same in all simulations.

[24] The temporal evolution of corresponding ring current parameters during 21–25 October 2001 is shown in Figure 5. Although W01 model predicted significant small-scale fluctuations in the CPCP drop not present in VS, both models showed maximum in the large-scale convection potential near hours ~24 and ~40. The first maximum was about 190 kV and was larger than the second one, which was ~140 kV using W01 (~170 kV using VS). This behavior was in good agreement with the CPCP derived from the polar cap index [*Troshichev et al.*, 1996]. The ring current injection rate during the main phase of the storm was about twice as large as using W01 versus using VS (Figure 5, middle panel) and resulted in a significantly stronger ring current. The first *Dst* minimum was thus well reproduced by the W01 convection model, while the VS model underestimated it by ~70 nT. (Note that the first, smaller, depression in *Dst* at hour ~22 predicted by the W01 model does appear in the high-time resolution SYM-H index shown in Figure 1.) The magnetopause current-correction to *Dst* after *Burton et al.* [1975] resulted in minimum *Dst* ~ −230 nT. The RAM model did not reproduce the magnetopause current-corrected *Dst*, confirming previous investigations that such correction is probably smaller than usually assumed during the main phase of large storms [*Siscoe et al.*, 2005]. Radial diffusion caused an additional enhancement of ring current injection rate near hour 48 and a ~20% increase in total ring current energy and ring current contribution to *Dst*. The second *Dst* minimum was thus better reproduced when W01 convection model including radial diffusion (solid line) was employed (Figure 5, bottom), but RAM still underestimated it by ~50 nT. Note that radial diffusion did not contribute significantly during the main phase of the storms.

[25] Contributions from substorm injections [e.g., *Ganushkina et al.*, 2000], magnetotail currents, and ring current electrons (not taken into account in this study) may bring better agreement with *Dst* observations on 22–23 October. Several sawtooth-like dipolarizations were observed by GOES 8, GOES 10, and LANL/MPA during 22 October which caused intensifications of the electron flux monitored by LANL/SOPA [*Pulkkinen et al.*, 2005; *Miyoshi et al.*, 2006]; furthermore, the GOES magnetotail field indicated that the cross-tail current was enhanced and its inner edge reached geosynchronous orbit. In addition, previous studies [e.g., *Jordanova and Miyoshi*, 2005; *Liu et al.*, 2005; *Miyoshi et al.*, 2006] have shown that the electron contribution to *Dst* is highly variable, being small (few %) during quiet times and the largest near *Dst* minima when it may contribute up to ~20% of the total ring current ion energy content. These contributions will be considered in future studies.

4.3. Comparison of Modeled Distributions With Satellite Data

[26] Distribution functions of H^+ and O^+ equatorially mirroring ($\alpha_o = 90°$) ions measured at several *L* shells with the Cluster/CIS spectrometer are shown as open squares in Figure 6. The data are obtained in the prenoon sector (MLT = 0900) near *Dst* minimum of the October 2001 storm. The distributions calculated with RAM using VS convection model (dashed), VS model and radial diffusion (dash-dotted), and W01 model and radial diffusion (solid) showed good overall agreement with the data except within the stagnation dip at ~10 keV. Radial diffusion injected high-energy particles and smoothed the gradients of the distribution functions, thus reducing the deep minima and improving the agreement with the data. Nevertheless, the VS convection model still underestimated the distributions inside the stagnation dip, and the W01 model reproduced better CIS data.

[27] Figure 7 shows a comparison of Polar/MICS H^+, He^+, and O^+ distribution functions (stars) with RAM calculations using VS convection model (dashed), VS

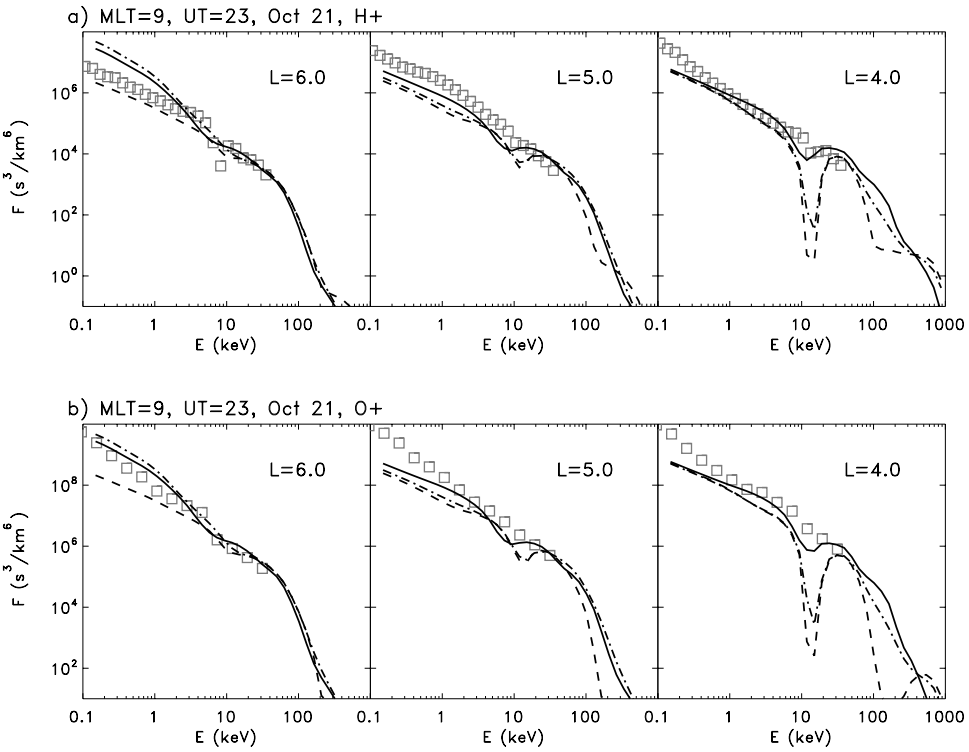

Figure 6. Comparison of (a) H^+ and (b) O^+ equatorially mirroring distributions (s^3 km^{-6}) calculated using Volland-Stern convection model (dashed line), Volland-Stern model and radial diffusion (dash-dotted line), or Weimer model and radial diffusion (solid line) with Cluster/CIS data (squares) during the storm main phase at 2300 UT on 21 October 2001 at different L shells and MLT = 0900.

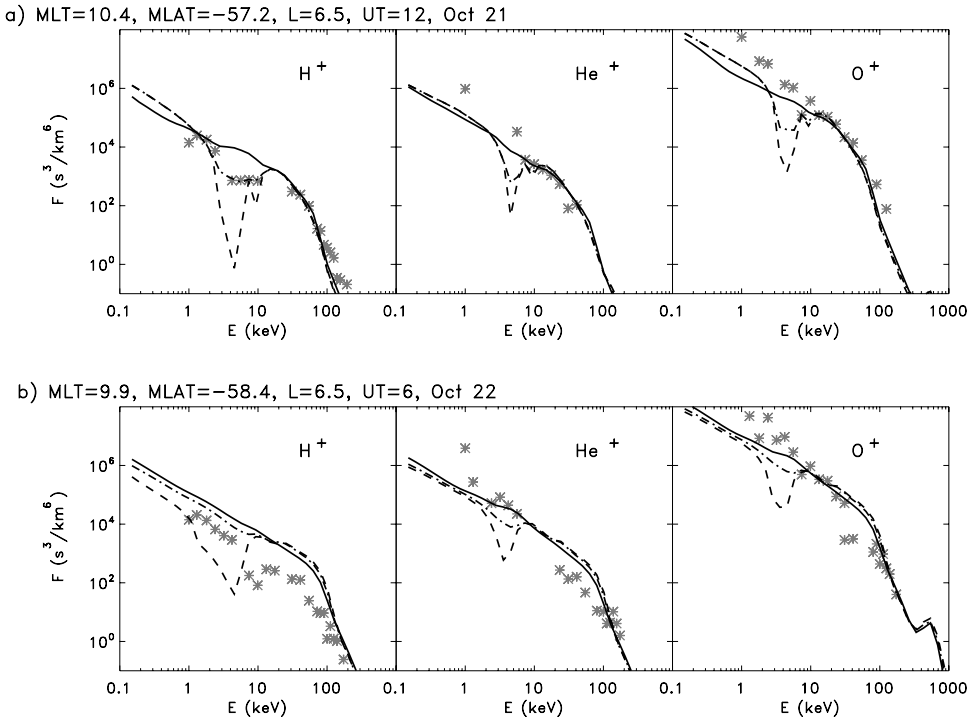

Figure 7. Comparison of H^+, He^+, and O^+ locally mirroring distributions (s^3 km^{-6}) at $L = 6.5$ calculated using Volland-Stern convection model (dashed line), Volland-Stern model and radial diffusion (dash-dotted line), or Weimer model and radial diffusion (solid line) with Polar/MICS data (stars) at (a) 1200 UT on 21 October and (b) 0600 UT on 22 October.

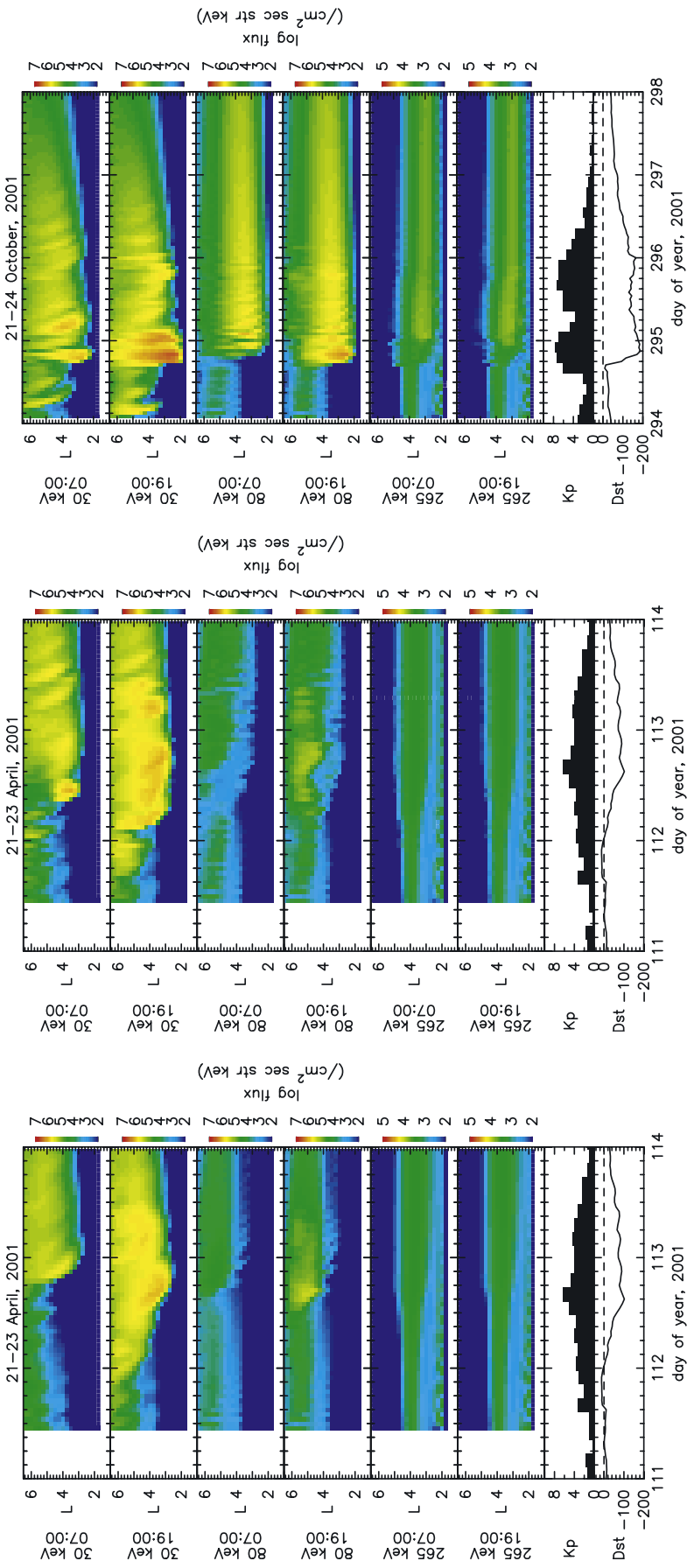
21–23 April, 2001
21–23 April, 2001
21–24 October, 2001
day of year, 2001
log flux
(/cm² sec str kev)
30 kev 07:00
30 kev 19:00
80 kev 07:00
80 kev 19:00
265 kev 07:00
265 kev 19:00
Kp
Dst

Figure 8

model and radial diffusion (dash-dotted), or Weimer model and radial diffusion (solid) during October 2001. Displayed are MICS locally mirroring distributions measured near minimum *Dst* when Polar was at high magnetic latitudes (MLAT) in the prenoon sector. To obtain locally mirroring distributions, the RAM distributions were mapped along magnetic field lines to the satellite position; they correspond to $\alpha_o \sim 7^\circ$ equatorial pitch angles. As in the comparison with CIS data, the VS model underestimated the values of the distributions within the stagnation dip, and adding radial diffusion improved the agreement with MICS data. There were no significant differences between the RAM simulations using the W01 model with or without (not shown) radial diffusion since there were no large dips predicted by the W01 model. These results are in agreement with previous studies [*Kistler et al.*, 1999; *Jordanova et al.*, 2001b] comparing modeled distributions with Equator-S/ESIC and Polar/HYDRA observations. These studies explained the wider dips obtained using the Volland-Stern rather than using the Weimer model, with differences in the drift velocities and drift paths of the ions; usually particles with small azimuthal velocity drifted at smaller distances from Earth in a VS model and thus underwent larger losses encountering higher geocoronal and plasmaspheric densities.

[28] Proton fluxes calculated with RAM during 21–23 April and 21–24 October 2001 are shown in Figure 8 in the same *L*-time format as NOAA data in Figure 2. We note that RAM fluxes correspond to $\alpha_o = 25^\circ$, while NOAA data correspond to variable pitch angles, so there may be differences in the flux magnitudes due to the different pitch angles sampled. From top to bottom are plotted 30 keV, 80 keV, and 265 keV fluxes at dawn (MLT = 0700) and dusk (MLT = 1900), respectively. As discussed by *Jordanova and Miyoshi* [2005], the fluxes at low energy (30 keV) were determined by magnetospheric convection, the fluxes at high energy (265 keV) were determined by radial diffusion, and the fluxes at intermediate energy (80 keV) were affected by both processes. A very asymmetric ring current population thus formed during the main phase of the storms at lower energies. In agreement with NOAA data, the fluxes were more intense near dusk than near dawn. The 30 keV fluxes penetrated deepest at dusk to $L = 2.5$ at ~1800 UT on 22 April using the VS convection model (Figure 8 left), and at ~0600 UT using the W01 convection model (Figure 8 middle). In comparison, NOAA data showed the deepest ion penetration during the storm main phase at ~1200 UT (Figure 2 left). Therefore the W01 (VS) model predicted earlier (later) ring current buildup than NOAA observations. This is demonstrated as well in the model predictions of *Dst* index during the April storm (Figure 4). During the October storm the 30 keV fluxes penetrated at dusk to $L = 2$ using the W01 model at ~1800 UT on 21 October (Figure 8 right) and at ~2400 UT using the VS model [*Jordanova and Miyoshi*, 2005]. NOAA data indicated deeper penetration at ~1800 UT in agreement with W01 model. This faster ring current buildup was again reflected in the sharp *Dst* decrease predicted well with W01 model (Figure 5). The ion enhancements at dawn occurred several hours later, the delay being bigger (~6 hours) using the VS model and smaller (~2–3 hours) using the W01 model. Similar trends were seen in the 80 keV fluxes, but their magnitude was significantly smaller. The highest energy (265 keV) fluxes were symmetric, being dominated by radial diffusion, although NOAA data exhibited some asymmetry even in this energy range.

4.4. Global Images of Trapped and Precipitating Fluxes

[29] To investigate the global morphology of the ring current population, we show differential fluxes of protons with $\alpha_o = 60^\circ$ and different energies near minimum *Dst* of the April and October 2001 storms in Figure 9 (left and right, respectively). At 1600 UT on 22 April the fluxes simulated with RAM were larger using the W01 convection model (Figure 9b) than using the VS model (Figure 9a). The 15 keV flux peaked in the postmidnight sector using either the VS or W01 models, while the 30 keV flux peaked in the premidnight sector using VS and near midnight using W01. By contrast at 0600 UT on 22 October, the 15 and 30 keV fluxes were larger using VS, and they peaked near midnight and dusk, respectively, while they peaked near midnight and near MLT ~ 0900 using W01 model. Radial diffusion did not cause any significant changes at these energies, and the ring current distribution remained asymmetric (Figure 9f). The 80 keV flux was larger using the W01 model because the small-scale fluctuations of W01 potential (Figure 5 top) contributed to the injection of high-energy particles. Figure 9c displays an initial RAM simulation using the W01 convection model and a self-consistently calculated magnetic field; more details about this calculation are presented by *Zaharia et al.* [2006]. It is clear that while the fluxes were reduced in magnitude, their global morphology was not changed significantly by the particle drifts in a nondipole magnetic field, and their peaks remained at approximately the same local time. Note that narrow pressure peaks and significantly enhanced plasma β did appear in localized regions on the nightside as discussed by *Zaharia et al.* [2006]. The storm-time intensification of the ring current depressed the inner magnetospheric magnetic field, which caused a subsequent reduction of about 20% of the total ring current energy (particles did not penetrate as deep and gained less energy due to the conservation of the first adiabatic invariant). It is clear from Figure 9 that the location of the flux peak in the equatorial plane was affected mainly by the morphology of the convection potential. *Denton et al.* [2005] made a detailed quantitative comparison of the location of the peak energetic neutral atom (ENA) flux at 6 and 12 keV predicted by either the VS or W01 convection models and IMAGE/MENA data during the October storm. They found

Figure 8. Calculated proton fluxes (1 cm^{-2} s^{-1} str^{-1} keV^{-1}) for three energy ranges and $\alpha_o = 25^\circ$ at MLT = 0700 and MLT = 1900, obtained with our model (left) using Volland-Stern model and radial diffusion, (middle) using Weimer model and radial diffusion, as a function of *L* shell and time during 21–23 April. (right) Proton fluxes obtained with RAM using Weimer model and radial diffusion during 21–24 October. The *Kp* and *Dst* indices are shown in the bottom panels for reference.

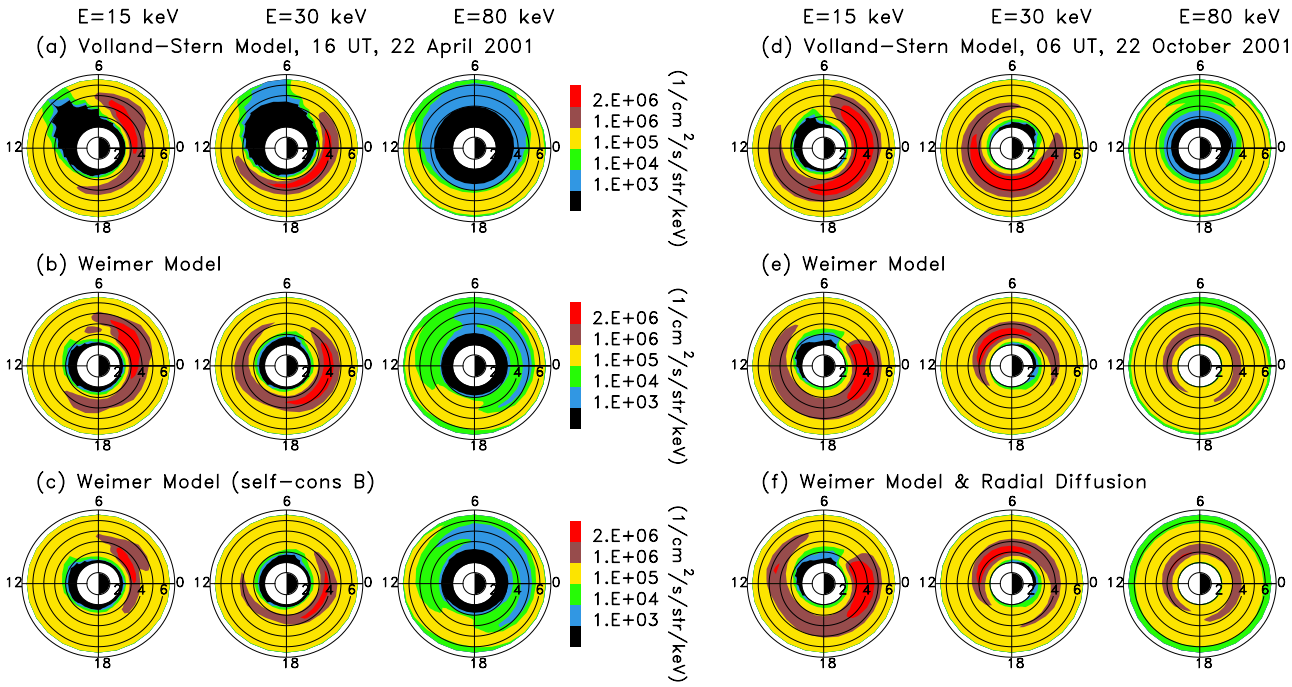

Figure 9. (left) Calculated proton number flux (1 cm^{-2} s^{-1} str^{-1} keV^{-1}) at three energies and $\alpha_o = 60°$, as a function of radial distance in the equatorial plane and MLT at 1600 UT on 22 April using (a) Volland-Stern model, (b) Weimer model, and (c) Weimer model and self-consistent calculations of the magnetic field. (right) Calculated proton number flux at 0600 UT on 22 October using (d) Volland-Stern model, (e) Weimer model, and (f) Weimer model and radial diffusion.

good agreement with the VS model predictions at 1800–2400 UT on 21 October, while the W01 model showed an ENA peak further duskward than observed. Ring current simulations using high-resolution convection potentials like W01 and AMIE [e.g., *Chen et al.*, 2003; *Jordanova et al.*, 2003] or self-consistently calculated electric field [e.g., *Wolf*, 1983; *Fok et al.*, 2003] predict variable location of the midenergy (30–80 keV) ion flux peaks during storm time. These electric potential models have quite irregular patterns that are distorted from simple dawn-dusk symmetric patterns exhibited by the analytical Volland-Stern model. The storm-time trajectories of the ring current particles are thus modified in these complex models and the peak location may occur from dusk to dawn. Another reason for the appearance of the flux peak at postmidnight during some storm times as seen by IMAGE data is the MLT dependence of the nightside plasma sheet ion density. During the 15 May 1997 storm, the ring current energy density peaked in the postmidnight sector even when a VS model was used [*Jordanova*, 2003], due to a localized enhancement of plasma sheet ion density at geosynchronous orbit during the storm main phase. The location of the peak depends as well on the ionospheric conductivity, which influences the intensity of the shielding electric field, since lower ionospheric conductivity results in a slightly eastward peak [*Wolf*, 1983; *Ebihara and Fok*, 2004].

[30] We calculated the growth rate of He^+ band EMIC waves self-consistently with the evolving ring current ion populations and show the results at selected hours during the April and October 2001 storms in Figure 10 (top). In these RAM simulations we used the W01 convection model and included radial diffusion. The regions of intense EMIC wave instability (wave gain larger than 40 dB) varied with time and were located either near the plasmapause or within high-density dayside plasmaspheric plumes. The wave activity maximized near minimum *Dst* and was stronger during the October storm due to the more intense ring current ion distributions (as reflected in the *Dst* indices) than during the April storm. Global distributions of precipitating (20–100 keV) proton flux calculated with RAM without or with plasma wave scattering are compared in the middle and bottom panels of Figure 10. The precipitating proton flux increases by several orders of magnitude within localized regions of large EMIC wave excitation, due to pitch angle diffusion of ring current protons into the atmospheric loss cone. Significant enhancements of precipitating fluxes thus occurred on 22 April in the postmidnight sector (Figure 10c), and on 22 October near dusk and in the postnoon sector (Figure 10f). We note that although the local effect of wave-particle interactions was substantial, this process led to only about 10% decrease of the total proton ring current energy during the storm recovery phase [*Jordanova*, 2005].

5. Summary and Conclusions

[31] We simulated the evolution of the inner magnetosphere during the 21–23 April and 21–25 October 2001 storm periods with our kinetic RAM model. The first time period represented a moderate geomagnetic storm with a gradual main phase and *Dst* minimum of about −100 nT, while the second was a large storm with a rapid main phase and a *Dst* minimum of about −190 nT. These storms have been investigated by the GEM/IMS campaign to assess our

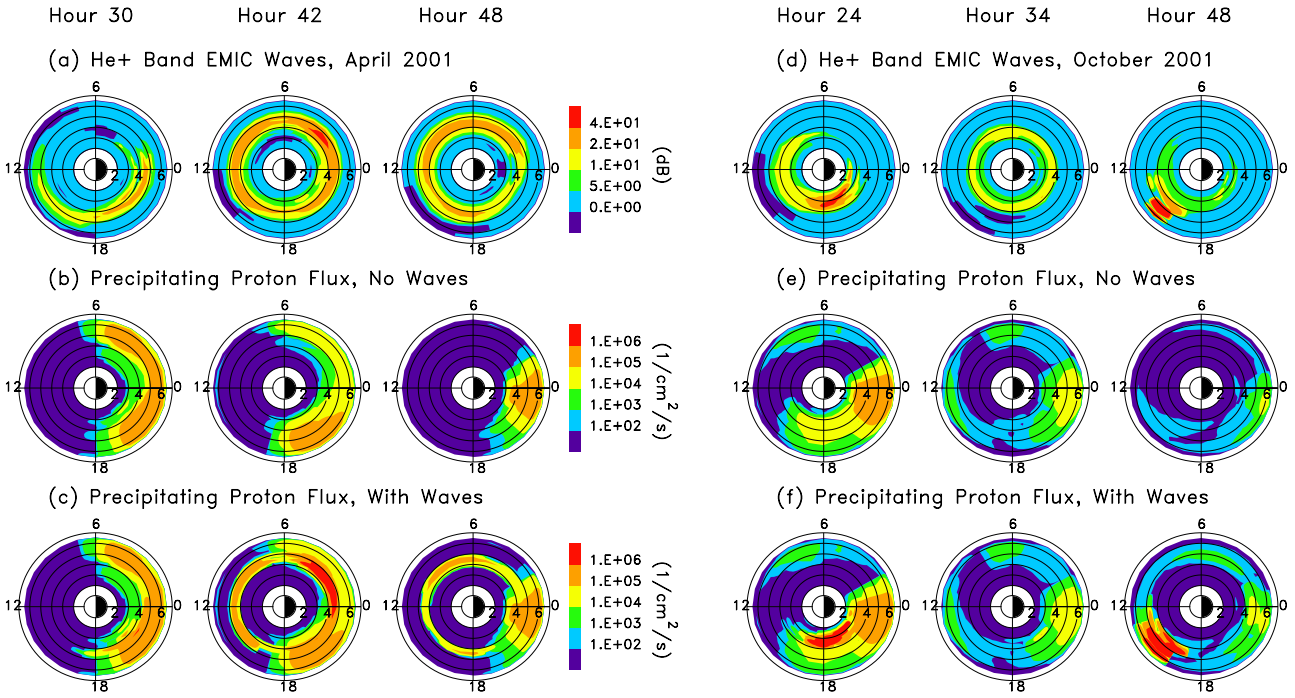

Figure 10. (top) Wave gain of He^+ band EMIC waves as a function of radial distance in the equatorial plane and MLT. Precipitating (20–100 keV) proton fluxes (middle) without and (bottom) with plasma wave scattering included, at selected hours after 0000 UT on 21 April (left) and after 0000 UT on 21 October (right).

understanding of the physics of the inner magnetosphere and the accuracy of present models in predicting geomagnetic storm dynamics. We compared results from our RAM model driven by an analytical VS [*Volland*, 1973; *Stern*, 1975; *Maynard and Chen*, 1975] convection model and a more complex empirical model of ionospheric potentials of *Weimer* [2001] and found:

[32] 1. Both VS and W01 models reproduced well the plasmapause location observed by IMAGE/EUV during less disturbed times and during the April storm. During active times the plasmapause was predicted at distances about 0.25 *L* shell larger than observed by IMAGE. The VS model predicted much better the plasmapause location during the October storm than W01.

[33] 2. The *Dst* minimum was significantly underestimated during both storms when VS model was used. The W01 model produced a larger injection rate and good agreement with the rapid ring current buildup during the October storm but underestimated its second *Dst* minimum as well as the *Dst* minimum on 22 April. Radial diffusion did not contribute to ring current buildup during the storm main phases but produced additional ion injections near *Dst* minima that improved the agreement with observations.

[34] 3. The comparison with Polar/MICS and Cluster/CIS in situ data during October 2001 showed that a *Kp*-dependent VS convection model underestimated the fluxes within the stagnation dip, especially at low *L* shells. Adding radial diffusion removed the sharp gradients and reduced the deep minima in the distribution functions. The W01 model showed good overall agreement with in situ data at all *L* shells.

[35] 4. The computed ion fluxes showed pronounced ring current asymmetry during the main phase of the storms in agreement with NOAA observations. Both convection models reproduced the enhancement of 30–80 keV fluxes near dusk, the enhancement with W01 model being faster and stronger. The 265 keV fluxes were determined by radial diffusion and were symmetric, while some asymmetry was still present in NOAA data. The overall RAM comparison with NOAA data was better during the October storm.

[36] 5. The location of the peak of the trapped (15–80 keV) H^+ fluxes in the equatorial plane varied during the storms depending on the convection electric field and plasma sheet density. The 15 keV flux peaked predominantly in the midnight-to-dawn sector in both models. The 30 keV flux peaked at dusk-to-midnight using VS and dusk-to-dawn using the W01 model. The 80 keV flux was larger using W01 than using VS model.

[37] 6. Initial results obtained from adding a self-consistently calculated magnetic field to RAM were presented for the April 2001 storm. The overall effect of including a self-consistent magnetic field calculation resulted in about a 20% reduction of the total ring current energy. While the global morphology of the ring current fluxes was not affected significantly, localized narrow pressure peaks appeared on the nightside, as discussed by *Zaharia et al.* [2006], who also found significant magnetic field depressions near Earth at the storm peak.

[38] 7. The precipitating (20–100 keV) H^+ fluxes also exhibited variable morphology during the storms. They intensified within localized regions of strong EMIC wave excitation near the plasmapause or inside plasmaspheric plumes. The wave activity was stronger during the October storm and caused ~10% reduction of the total H^+ energy.

[39] In conclusion, the RAM model reproduced reasonably well the ring current ion buildup and decay during the

April and October 2001 storms. In general, the W01 convection model reproduced better the ring current dynamics and the *Dst* index, while the VS model reproduced better the storm-time dynamics of the plasmasphere and the evolution of the plasmapause. The *Kp*-dependent version of the VS model we used was derived using plasmapause observations to determine the strength of the convection [*Maynard and Chen*, 1975] and showed indeed very good agreement with IMAGE plasmapause observations. Further improvements of the empirical electric field models are needed to more accurately reproduce the dynamics of both cold and hot plasma populations in the inner magnetosphere. Future extensions of this work will consider full coupling between RAM and the three-dimensional equilibrium code of *Zaharia et al.* [2004], as well as incorporation of a self-consistent calculation of the electric field in RAM. The self-consistently computed magnetic field will be applied to study the dynamics of radiation belt electrons during geomagnetic storms, a topic of high interest to the national space weather program.

[40] **Acknowledgments.** This work was supported by NASA grants NAG5-13512 and NNG05GG50G, and NSF grant ATM-0309585. Work at Los Alamos was conducted under the auspices of the U. S. Department of Energy, with partial support from the NASA Living With a Star TR&T program, and from a Los Alamos National Laboratory Directed Research and Development grant. The work at STEL, Nagoya University was supported by grant-in-aid for scientific research (17740326) from the Ministry of Education, Science, Sports and Culture, Japan. The work at Aerospace was supported in part by grant GC190056NGA. We would like to thank J. Goldstein for making IMAGE/EUV data available for the GEM challenge events. ACE data were provided by D. McComas and N. Ness through the CDAWeb at NASA. The *Dst* and SYM-H indices were provided by the World Data Center in Kyoto, Japan.

[41] Amitava Bhattacharjee thanks Mostafa El-Alaoui and Colby Lemon for their assistance in evaluating this paper.

References

Belian, R. D., G. R. Gisler, T. Cayton, and R. Christensen (1992), High-Z energetic particles at geosynchronous orbit during the great solar proton event series of October 1989, *J. Geophys. Res.*, *97*, 16,897.

Brautigam, D. H., and J. M. Albert (2000), Radial diffusion analysis of outer radiation belt electrons during the October 9, 1990, magnetic storm, *J. Geophys. Res.*, *105*, 291.

Burton, R. K., R. L. McPherron, and C. T. Russell (1975), An empirical relationship between interplanetary conditions and *Dst*, *J. Geophys. Res.*, *80*, 4204.

Chen, M. W., L. R. Lyons, and M. Schulz (1994), Simulations of phase space distributions of storm time proton ring current, *J. Geophys. Res.*, *99*, 5745.

Chen, M. W., M. Schulz, G. Lu, and L. R. Lyons (2003), Quasi-steady drift paths in a model magnetosphere with AMIE electric field: Implications for ring current formation, *J. Geophys. Res.*, *108*(A5), 1180, doi:10.1029/2002JA009584.

Denton, M. H., V. K. Jordanova, M. G. Henderson, R. M. Skoug, M. F. Thomsen, C. J. Pollock, S. Zaharia, and H. O. Funsten (2005), Storm-time plasma signatures observed by IMAGE/MENA and comparison with a global physics-based model, *Geophys. Res. Lett.*, *32*, L17102, doi:10.1029/2005GL023353.

Dessler, A. J., and E. N. Parker (1959), Hydromagnetic theory of geomagnetic storms, *J. Geophys. Res.*, *64*, 2239.

De Zeeuw, D. L., S. Sazykin, R. A. Wolf, T. I. Gombosi, A. J. Ridley, and G. Toth (2004), Coupling of a global MHD code and an inner magnetospheric model: Initial results, *J. Geophys. Res.*, *109*, A12219, doi:10.1029/2003JA010366.

Ebihara, Y., and M. C. Fok (2004), Postmidnight storm-time enhancement of tens-of-keV proton flux, *J. Geophys. Res.*, *109*, A12209, doi:10.1029/2004JA010523.

Evans, D. S., and M. S. Greer (2000), Polar orbiting environmental satellite space environment monitor: 2. Instrument description and archive data documentation, *Tech. Memo. OAR SEC-93*, NOAA, Boulder, Colo.

Fok, M.-C., J. U. Kozyra, A. F. Nagy, C. E. Rasmussen, and G. V. Khazanov (1993), Decay of equatorial ring current ions and associated aeronomical consequences, *J. Geophys. Res.*, *98*, 19,381.

Fok, M.-C., R. A. Wolf, R. W. Spiro, and T. E. Moore (2001), Comprehensive computational model of the Earth's ring current, *J. Geophys. Res.*, *106*, 8417.

Fok, M.-C., et al. (2003), Global ENA image simulations, *Space Sci. Rev.*, *109*, 77.

Ganushkina, N. Y., et al. (2000), Entry of plasma sheet particles into the inner magnetosphere as observed by Polar/CAMMICE, *J. Geophys. Res.*, *105*, 25,205.

Goldstein, J., B. R. Sandel, W. T. Forrester, M. F. Thomsen, and M. R. Hairston (2005), Global plasmasphere evolution 22–23 April 2001, *J. Geophys. Res.*, *110*, A12218, doi:10.1029/2005JA011282.

Jordanova, V. K. (2003), New insights on geomagnetic storms from model simulations using multi-spacecraft data, *Space Sci. Rev.*, *107*, 157.

Jordanova, V. K. (2005), Sources, transport, and losses of energetic particles during geomagnetic storms, in *The Inner Magnetosphere: Physics and Modeling*, *Geophys. Monogr. Ser.*, vol. 155, edited by T. I. Pulkkinen, N. A. Tsyganenko, and R. H. W. Friedel, p. 9, AGU, Washington, D. C.

Jordanova, V. K., and Y. Miyoshi (2005), Relativistic model of ring current and radiation belt ions and electrons: Initial results, *Geophys. Res. Lett.*, *32*, L14104, doi:10.1029/2005GL023020.

Jordanova, V. K., J. U. Kozyra, G. V. Khazanov, A. F. Nagy, C. E. Rasmussen, and M.-C. Fok (1994), A bounce-averaged kinetic model of the ring current ion population, *Geophys. Res. Lett.*, *21*, 2785.

Jordanova, V. K., L. M. Kistler, J. U. Kozyra, G. V. Khazanov, and A. F. Nagy (1996a), Collisional losses of ring current ions, *J. Geophys. Res.*, *101*, 111.

Jordanova, V. K., J. U. Kozyra, and A. F. Nagy (1996b), Effects of heavy ions on the quasi-linear diffusion coefficients from resonant interactions with EMIC waves, *J. Geophys. Res.*, *101*, 19,771.

Jordanova, V. K., C. J. Farrugia, R. M. Thorne, G. V. Khazanov, G. D. Reeves, and M. F. Thomsen (2001a), Modeling ring current proton precipitation by electromagnetic ion cyclotron waves during the May 14–16, 1997, storm, *J. Geophys. Res.*, *106*, 7.

Jordanova, V. K., L. M. Kistler, C. J. Farrugia, and R. B. Torbert (2001b), Effects of inner magnetospheric convection on ring current dynamics: March 10–12, 1998, *J. Geophys. Res.*, *106*, 29,705.

Jordanova, V. K., A. Boonsiriseth, R. M. Thorne, and Y. Dotan (2003), Ring current asymmetry from global simulations using a high-resolution electric field model, *J. Geophys. Res.*, *108*(A12), 1443, doi:10.1029/2003JA009993.

Jordanova, V. K., C. G. Mouikis, L. M. Kistler, H. Matsui, P. Puhl-Quinn and Y. Khotyaintsev (2005), Storm time ring current-atmosphere interactions: Observations and modeling, in *Cluster and Double Star Symposium: Fifth Anniversary of Cluster in Space*, edited by K. Fletcher, *Eur. Space Agency Spec. Publ.*, *ESA SP-598*.

Kistler, L. M., F. M. Ipavich, D. C. Hamilton, G. Gloeckler, B. Wilken, G. Kremser, and W. Stuedemann (1989), Energy spectra of the major ion species in the ring current during geomagnetic storms, *J. Geophys. Res.*, *94*, 3579.

Kistler, L. M., et al. (1999), Testing electric field models using ring current ion energy spectra from the Equator-S ion composition (ESIC) instrument, *Ann. Geophys.*, *17*, 1611.

Lemon, C., R. A. Wolf, T. W. Hill, S. Sazykin, R. W. Spiro, F. R. Toffoletto, J. Birn, and M. Hesse (2004), Magnetic storm ring current injection modeled with the Rice Convection Model and a self-consistent magnetic field, *Geophys. Res. Lett.*, *31*, L21801, doi:10.1029/2004GL020914.

Lennartsson, W., E. G. Shelley, R. D. Sharp, R. G. Johnson, and H. Balsiger (1979), Some initial ISEE-1 results on the ring current composition and dynamics during the magnetic storm of December 11, 1977, *Geophys. Res. Lett.*, *6*, 483.

Liemohn, M. W., A. J. Ridley, D. L. Gallagher, D. M. Ober, and J. U. Kozyra (2004), Dependence of plasmaspheric morphology on the electric field description during the recovery phase of the 17 April 2002 magnetic storm, *J. Geophys. Res.*, *109*, A03209, doi:10.1029/2003JA010304.

Liu, S., M. W. Chen, J. L. Roeder, L. R. Lyons, and M. Schulz (2005), Relative contribution of electrons to the stormtime total ring current energy content, *Geophys. Res. Lett.*, *32*, L03110, doi:10.1029/2004GL021672.

Maynard, N. C., and A. J. Chen (1975), Isolated cold plasma regions: Observations and their relation to possible production mechanisms, *J. Geophys. Res.*, *80*, 1009.

McComas, D. J., S. J. Bame, B. L. Barraclough, J. R. Donart, R. C. Elphic, J. T. Gosling, M. B. Moldwin, K. R. Moore, and M. F. Thomsen (1993), Magnetospheric plasma analyzer: Initial three-spacecraft observations from geosynchronous orbit, *J. Geophys. Res.*, *98*, 13,453.

McComas, D. J., S. J. Bame, P. Barker, W. C. Feldman, J. L. Phillips, P. Riley, and J. W. Griffee (1998), Solar wind electron proton alpha monitor (SWEPAM) for the advanced composition explorer, *Space Sci. Rev.*, *86*, 563.

Miyoshi, Y. S., V. K. Jordanova, A. Morioka, M. F. Thomsen, G. D. Reeves, D. S. Evans, and J. C. Green (2006), Observations and modeling of energetic electron dynamics during the Oct. 2001 storm, *J. Geophys. Res.*, *111*, A11S02, doi:10.1029/2005JA011351.

O'Brien, T. P., and M. B. Moldwin (2003), Empirical plasmapause models from magnetic indices, *Geophys. Res. Lett.*, *30*(4), 1152, doi:10.1029/2002GL016007.

Pulkkinen, T. I., N. Ganushkina, E. Donovan, X. Li, G. Reeves, C. Russell, H. Singer, and J. Slavin (2005), Storm-substorm coupling during 16 hours of *Dst* steadily at −150 nT, in *The Inner Magnetosphere: Physics and Modeling*, *Geophys. Monogr. Ser.*, vol. 155, edited by T. I. Pulkkinen, N. A. Tsyganenko, and R. H. W. Friedel, p. 155, AGU, Washington, D. C.

Rasmussen, C. E., S. M. Guiter, and S. G. Thomas (1993), Two-dimensional model of the plasmasphere: Refilling time constants, *Planet. Space Sci.*, *41*, 35.

Rème, H., et al. (2001), First multispacecraft ion measurements in and near the Earth's magnetosphere with the identical Cluster ion spectrometry (CIS) experiment, *Ann. Geophys.*, *19*, 1303.

Ridley, A. J., T. I. Gombosi, and D. L. De Zeeuw (2004), Ionospheric control of the magnetosphere: Conductance, *Ann. Geophys.*, *22*, 567.

Roederer, J. G. (1970), *Dynamics of Geomagnetically Trapped Radiation*, Springer, New York.

Sandel, B. R., R. A. King, W. T. Forrester, D. L. Gallagher, A. L. Broadfoot, and C. C. Curtis (2001), Initial results from the IMAGE extreme ultraviolet imager, *Geophy. Res. Lett.*, *28*, 1439.

Schulz, M., and L. J. Lanzerotti (1974), *Particle Diffusion in the Radiation Belts*, Springer, New York.

Sckopke, N. (1966), A general relation between the energy of trapped particles and the disturbance field over the Earth, *J. Geophys. Res.*, *71*, 3125.

Shprits, Y. Y., and R. M. Thorne (2004), Time dependent radial diffusion modeling of relativistic electrons with realistic loss rates, *Geophys. Res. Lett.*, *31*, L08805, doi:10.1029/2004GL019591.

Shukhtina, M. A. (1993), On the calculation of magnetic drift velocity of particles with arbitrary pitch angles, *Planet. Space Sci.*, *41*, 327.

Sibeck, D. G., R. W. McEntire, A. T. Y. Lui, R. E. Lopez, and S. M. Krimigis (1987), Magnetic field drift shell splitting: Cause of unusual dayside particle pitch angle distributions during storms and substorms, *J. Geophys. Res.*, *92*, 13,485.

Siscoe, G. L., R. L. McPherron, and V. K. Jordanova (2005), Diminished contribution of ram pressure to Dst during magnetic storms, *J. Geophys. Res.*, *110*, A12227, doi:10.1029/2005JA011120.

Smith, C. W., J. L'Heureux, N. F. Ness, M. H. Acuna, L. F. Burlaga, and J. Scheifele (1998), The ACE magnetic fields experiment, *Space Sci. Rev.*, *86*, 613.

Stern, D. P. (1975), The motion of a proton in the equatorial magnetosphere, *J. Geophys. Res.*, *80*, 595.

Toffoletto, F., S. Sazykin, R. Spiro, and R. Wolf (2003), Inner magnetospheric modeling with the Rice Convection Model, *Space Sci. Rev.*, *107*, 175.

Troshichev, O., H. Hayakawa, A. Matsuoka, T. Mukai, and K. Tsuruda (1996), Cross polar cap diameter and voltage as a function of PC index and interplanetary quantities, *J. Geophys. Res.*, *101*, 13,429.

Tsyganenko, N. A. (2002), A model of the magnetosphere with a dawn-dusk asymmetry: 1. Mathematical structure, *J. Geophys. Res.*, *107*(A8), 1179, doi:10.1029/2001JA000219.

Vapirev, A., and V. K. Jordanova (2005), Calculation of bounce-averaged velocities and Hydrogen densities for a non-dipole magnetic field, *Eos Trans. AGU*, *86*(52), Fall Meet. Suppl., Abstract SM41A-1162.

Volland, H. (1973), A semiempirical model of large-scale magnetospheric electric fields, *J. Geophys. Res.*, *78*, 171.

Weimer, D. R. (1996), A flexible, IMF dependent model of high-latitude electric potentials having "space weather" applications, *Geophys. Res. Lett.*, *23*, 2549.

Weimer, D. R. (2001), An improved model of ionospheric electric potentials including substorm perturbations and application to the Geospace Environment Modeling November 24, 1996, event, *J. Geophys. Res.*, *106*, 407.

Wilken, B., W. Weiss, D. Hall, M. Grande, F. Soraas, and J. F. Fennell (1992), Magnetospheric ion composition spectrometer onboard the CRRES spacecraft, *J. Spacecr. Rockets*, *29*, 585.

Wolf, R. A. (1983), The quasi-static (slow-flow) region of the magnetosphere, in *Solar Terrestrial Physics*, edited by R. L. Carovillano and J. M. Forbes, p. 303, Springer, New York.

Wolf, R. A., M. Harel, R. W. Spiro, G. Voigt, P. H. Reiff, and C. K. Chen (1982), Computer simulation of inner magnetospheric dynamics for the magnetic storm of July 29, 1977, *J. Geophys. Res.*, *87*, 5949.

Young, D. T., H. Balsiger, and J. Geiss (1982), Correlations of magnetospheric ion composition with geomagnetic and solar activity, *J. Geophys. Res.*, *87*, 9077.

Zaharia, S., C. Z. Cheng, and K. Maezawa (2004), 3-D force-balanced magnetospheric configurations, *Ann. Geophys.*, *22*, 251, doi:1432-0576/ag/2004-22-251.

Zaharia, S., M. F. Thomsen, J. Birn, M. H. Denton, V. K. Jordanova, and C. Z. Cheng (2005), Effect of storm-time plasma pressure on the magnetic field in the inner magnetosphere, *Geophys. Res. Lett.*, *32*, L03102, doi:10.1029/2004GL021491.

Zaharia, S., V. K. Jordanova, M. F. Thomsen, and G. D. Reeves (2006), Self-consistent modeling of magnetic fields and plasmas in the inner magnetosphere: Application to a geomagnetic storm, *J. Geophys. Res.*, *111*, A11S14, doi:10.1029/2006JA011619.

D. S. Evans, Space Environment Center, NOAA, Boulder, CO 80305, USA.

J. F. Fennell, The Aerospace Corporation, Los Angeles, CA 90009, USA.

V. K. Jordanova, G. D. Reeves, M. F. Thomsen, and S. Zaharia, Los Alamos National Laboratory, Los Alamos, NM 87545, USA. (vania@lanl.gov)

Y. S. Miyoshi, Solar-Terrestrial Environment Laboratory, Nagoya University, Nagoya 464-8601, Japan.

C. G. Mouikis, Space Science Center, University of New Hampshire, 39 College Road, Durham, NH 03824, USA.